Journal of Nuclear Medicine, published on February 11, 2010 as doi:10.2967/jnumed.109.068007

Targeted Contrast-Enhanced Ultrasound Imaging of Tumor Angiogenesis with Contrast Microbubbles Conjugated to Integrin-Binding Knottin Peptides

Jürgen K. Willmann[1], Richard H. Kimura[1,2], Nirupama Deshpande[1], Amelie M. Lutz[1], Jennifer R. Cochran[2], and Sanjiv S. Gambhir[1,2]

[1]*Molecular Imaging Program at Stanford, Department of Radiology, School of Medicine, Stanford University, Stanford, California; and* [2]*Department of Bioengineering, School of Medicine, Stanford University, Stanford, California*

Targeted contrast-enhanced ultrasound imaging is increasingly being recognized as a powerful imaging tool for the detection and quantification of tumor angiogenesis at the molecular level. The purpose of this study was to develop and test a new class of targeting ligands for targeted contrast-enhanced ultrasound imaging of tumor angiogenesis with small, conformationally constrained peptides that can be coupled to the surface of ultrasound contrast agents. **Methods:** Directed evolution was used to engineer a small, disulfide-constrained cystine knot (knottin) peptide that bound to $\alpha_v\beta_3$ integrins with a low nanomolar affinity ($Knottin_{Integrin}$). A targeted contrast-enhanced ultrasound imaging contrast agent was created by attaching $Knottin_{Integrin}$ to the shell of perfluorocarbon-filled microbubbles ($MB\text{-}Knottin_{Integrin}$). A knottin peptide with a scrambled sequence was used to create control microbubbles ($MB\text{-}Knottin_{Scrambled}$). The binding of $MB\text{-}Knottin_{Integrin}$ and $MB\text{-}Knottin_{Scrambled}$ to $\alpha_v\beta_3$ integrin-positive cells and control cells was assessed in cell culture binding experiments and compared with that of microbubbles coupled to an anti-$\alpha_v\beta_3$ integrin monoclonal antibody ($MB_{\alpha v\beta 3}$) and microbubbles coupled to the peptidomimetic agent c(RGDfK) (MB_{cRGD}). The in vivo imaging signals of contrast-enhanced ultrasound with the different types of microbubbles were quantified in 42 mice bearing human ovarian adenocarcinoma xenograft tumors by use of a high-resolution 40-MHz ultrasound system. **Results:** $MB\text{-}Knottin_{Integrin}$ attached significantly more to $\alpha_v\beta_3$ integrin-positive cells (1.76 ± 0.49 [mean ± SD] microbubbles per cell) than to control cells (0.07 ± 0.006). Control $MB\text{-}Knottin_{Scrambled}$ adhered less to $\alpha_v\beta_3$ integrin-positive cells (0.15 ± 0.12) than $MB\text{-}Knottin_{Integrin}$. After blocking of integrins, the attachment of $MB\text{-}Knottin_{Integrin}$ to $\alpha_v\beta_3$ integrin-positive cells decreased significantly. The in vivo ultrasound imaging signal was significantly higher after the administration of $MB\text{-}Knottin_{Integrin}$ than after the administration of $MB_{\alpha v\beta 3}$ or control $MB\text{-}Knottin_{Scrambled}$. After in vivo blocking of integrin receptors, the imaging signal after the administration of $MB\text{-}Knottin_{Integrin}$ decreased significantly (by 64%). The imaging signals after the administration of $MB\text{-}Knottin_{Integrin}$ were not significantly different in the groups of tumor-bearing mice imaged with $MB\text{-}Knottin_{Integrin}$ and with MB_{cRGD}. Ex vivo immunofluorescence confirmed integrin expression on endothelial cells of human ovarian adenocarcinoma xenograft tumors. **Conclusion:** Integrin-binding knottin peptides can be conjugated to the surface of microbubbles and used for in vivo targeted contrast-enhanced ultrasound imaging of tumor angiogenesis. Our results demonstrate that microbubbles conjugated to small peptide-targeting ligands provide imaging signals higher than those provided by a large antibody molecule.

Key Words: targeted ultrasound imaging; contrast-enhanced ultrasound imaging; ovarian cancer; knottin peptides

J Nucl Med 2010; 51:433–440
DOI: 10.2967/jnumed.109.068007

Targeted contrast-enhanced ultrasound imaging with gas-filled echogenic microbubbles as contrast agents is increasingly being recognized as a promising and powerful molecular imaging tool (*1*). Ultrasound contrast agents can be targeted to specific molecular markers through the attachment of appropriate ligands to the surface of the microbubbles. After intravenous injection, these functionalized microbubbles attach at tissue sites expressing the target molecular marker, leading to a local increase in the ultrasonic imaging signal. Because of their size (several micrometers), currently available contrast microbubbles stay predominantly within the vascular system (*2*). This feature makes targeted contrast-enhanced ultrasound imaging exquisitely attractive as a noninvasive imaging tool for detecting and tracking biologic processes on vascular endothelial cells, such as tumor angiogenesis.

In tumor angiogenesis, which is the formation and recruitment of new blood vessels from the surrounding host tissue, various molecular markers are overexpressed on tumor vascular endothelial cells (*3,4*). These molecular markers are involved in the regulation and maintenance of

Received Jul. 6, 2009; revision accepted Dec. 10, 2009.
For correspondence or reprints contact: Jürgen K. Willmann, Molecular Imaging Program at Stanford, Department of Radiology, School of Medicine, Stanford University, 300 Pasteur Dr., Room H1307, Stanford, CA 94305-5105.
E-mail: willmann@stanford.edu

an angiogenic phenotype that is needed in many tumors to maintain a sufficient supply of oxygen, nutrients, and other growth factors. Among others, integrins are well-characterized molecular markers of tumor angiogenesis. Integrins are a class of heterodimeric cell surface adhesion receptors that are overexpressed on tumor endothelial cells during tumor angiogenesis. They bind to extracellular matrix proteins such as fibronectin, fibrinogen, von Willebrand factor, vitronectin, and proteolysis-generated forms of collagen and laminin, which promote cell adhesion to the extracellular matrix and activation of signaling pathways involved in tumor cell growth, invasion, and metastasis (*5*). In particular, $\alpha_v\beta_3$ integrin is highly expressed on activated angiogenic endothelial cells in tumor vessels, resulting in cancers that are more invasive, more migratory, and better able to survive in different microenvironments (*6*). Therefore, noninvasive imaging strategies for the detection and quantification of $\alpha_v\beta_3$ integrin may be particularly helpful for diagnosing cancer at early stages, developing anticancer therapeutic agents in preclinical animal models, and monitoring antiangiogenic and tumoricidal treatments in cancer patients.

Recent studies showed the feasibility of targeted contrast-enhanced ultrasound imaging of tumor angiogenesis with different commercially available integrin-targeting ligands, such as peptidomimetic agents, monoclonal antibodies, or echistatin (*7–9*). In the present proof-of-principle study, we tested whether engineered cystine knot (knottin) peptides could be coupled to the surface of contrast microbubbles and used as a new class of targeting ligands for targeted contrast-enhanced ultrasound imaging of tumor angiogenesis. Knottin peptides are small peptides (30–40 amino acids) containing conformationally constrained loop structures that naturally bind to a wide variety of targets (*10*). Previously, directed evolution was used to engineer the surface-exposed trypsin-binding loop of the *Ecballium elaterium* trypsin inhibitor II knottin peptide (*11*) to bind to tumor-specific integrin receptors with a low nanomolar affinity (*12*). Here, we chemically coupled this integrin-binding knottin peptide to the surface of contrast microbubbles and assessed their ability to bind to tumor cells expressing $\alpha_v\beta_3$ integrin and their ability to be used as ultrasound contrast agents for human subcutaneous ovarian cancer xenograft tumors in living mice. We compared our results with those obtained with microbubbles conjugated to an integrin-binding peptidomimetic agent or an antiintegrin monoclonal antibody. Our study validates knottin peptides as a general class of ligands for targeted ultrasound with contrast microbubbles and demonstrates that knottin peptides engineered against other molecular targets besides integrins hold much promise for molecular imaging applications.

MATERIALS AND METHODS

Synthesis of Integrin-Binding Ligand ($Knottin_{Integrin}$)

An engineered knottin peptide ($Knottin_{Integrin}$) containing the sequence GCPQGRGDWAPTSCCSQDSDCLAGCVCGPNGFCG was synthesized on a CS336 sold-phase peptide synthesizer (CS Bio Co.) by 9-fluorenylmethyloxycarbonyl chemistry using Rink amide resin (CS Bio Co.). 9-Fluorenylmethyloxycarbonyl groups on protected amino acids (Novabiochem/EMD Chemicals Inc.) were removed with 20% piperidine in *N,N*-dimethylformamide. Amino acid coupling was performed with *N*-hydroxybenzotriazole and diisopropylcarbodiimide in *N,N*-dimethylformamide. After synthesis, side-chain deprotection and resin cleavage were achieved by the addition of a 94:2.5:2.5:1 (v/v) mixture of trifluoroacetic acid:triisopropylsilane:ethanedithiol:water for 2 h at room temperature.

Crude peptide was purified by reversed-phase high-performance liquid chromatography (HPLC) with a Varian Prostar instrument (Varian, Inc.), a Vydac C_{18} column (Grace/Vydac), and a linear gradient composed of 90% acetonitrile in water containing 0.1% (v/v) trifluoroacetic acid. Folding reactions were performed by incubating the peptide overnight with 2.5 mM reduced glutathione and 20% (v/v) dimethyl sulfoxide in 0.1 M ammonium bicarbonate (pH 9). The folded knottin peptide was purified by reversed-phase HPLC as described earlier and site specifically biotinylated at its N terminus for conjugation to the microbubble shell. For this purpose, a molar excess of EZ-Link NHS-PEO_4-Biotin (Pierce Chemical Co.) was reacted overnight with purified $Knottin_{Integrin}$ in phosphate-buffered saline (PBS, pH 8). The resulting bioconjugate was purified by reversed-phase HPLC, and the molecular mass was determined by matrix-assisted laser desorption ionization–time-of-flight mass spectrometry ($[M+H]^+$, 3,678.01 Da). Peptide concentrations were determined by amino acid analysis (AAA Service Laboratory).

A knottin peptide ($Knottin_{Scrambled}$) containing a scrambled RGD sequence (GCVTGRDGSPASSCCSQDSDCLAGCVCGPNGFCG) was also synthesized and biotinylated as described earlier for use as a negative control.

Preparation of Microbubbles

$Knottin_{Integrin}$ was coupled to commercially available lipid-shelled, perfluorocarbon-containing microbubbles through streptavidin–biotin interactions (MicroMarker contrast agents; VisualSonics). The size (mean ± SD) of the microbubbles was 1.5 ± 0.1 μm (range, 1–2 μm), as assessed by use of a cell counter and sizer (Multisizer III Coulter Counter; Beckman Coulter). As a negative control, biotinylated $Knottin_{Scrambled}$ was also coupled to microbubbles for analysis. Two additional types of microbubbles were prepared: microbubbles coupled to a biotinylated rat antimouse $\alpha_v\beta_3$ integrin monoclonal antibody (eBioscience) ($MB_{\alpha v\beta 3}$) and microbubbles coupled to biotinylated c(RGDfK), an $\alpha_v\beta_3$ integrin-binding pentapeptide (Peptides International) (MB_{cRGD}). All ligands were added in excess amounts (10 μg) to occupy all binding sites on the microbubble surface. Unbound ligand remaining after microbubble conjugation was removed by centrifuging the reaction mixture at 300*g* for 2 min, and microbubble-containing supernatant was collected and reconstituted in saline. This washing procedure was repeated 2 times. On the basis of the assumption of complete surface conjugation, the average number of binding ligands per square micrometer of the microbubble surface was approximately 7,600.

Cell Lines

For cell culture experiments, $\alpha_v\beta_3$ integrin-positive mouse angiosarcoma endothelial cells (SVR) were grown in a high concentration of glucose (4.5 g/L) in Dulbecco modified Eagle

medium with L-glutamine (Invitrogen), and $\alpha_v\beta_3$ integrin-negative mouse breast cancer cells (4T1; American Type Culture Collection) were grown in RPMI 1640 medium (Invitrogen). For in vivo mouse experiments, human ovarian adenocarcinoma (SKOV-3) cells were grown in McCoy 5A medium (Invitrogen). All media were supplemented with 10% fetal bovine serum, penicillin (100 U/mL), and streptomycin (100 μg/mL).

Flow Chamber Cell Attachment Studies

To test the specificity of binding of the various microbubbles to mouse $\alpha_v\beta_3$ integrin, 5×10^4 integrin-positive (SVR) and integrin-negative (4T1) cells were grown on cover slips and mounted on a parallel-plate flow chamber (GlycoTech Corp.). In separate experiments, MB-Knottin$_{Integrin}$, MB-Knottin$_{Scrambled}$, MB$_{\alpha v\beta 3}$, or MB$_{cRGD}$ at a concentration of 0.7×10^7 microbubbles per milliliter in PBS was passed over the cells by use of a syringe infusion/withdrawal pump (Genie Plus; Kent Scientific Corp.) at a flow rate of 0.6 mL/min (corresponding to a wall shear rate of 100 s^{-1}, the approximate shear rate in tumor capillaries). This step was followed by a 2-min PBS rinse at the same flow rate. The mean number of microbubbles attached per cell in 5 randomly selected optical fields was determined by microscopy (at ×400; Axiovert 25; Carl Zeiss AG). Microbubbles can be directly visualized as small, rounded structures; microbubbles were considered to be attached to cells when there was direct contact with the cells and no evidence of free floating. The number of attached microbubbles and the number of cells were counted to calculate the number of attached microbubbles per cell (*13*). To further test the binding specificity of MB-Knottin$_{Integrin}$, integrin-positive cells were preincubated with an excess of c(RGDyK) pentapeptide (1.25 μmol/μl) to block integrin-binding sites before analysis. Experiments were performed in triplicate.

Small-Animal Imaging Experiments

Mouse Tumor Models. Animal protocols were approved by the Institutional Administrative Panel on Laboratory Animal Care of Stanford University. Subcutaneous human ovarian adenocarcinoma xenograft tumors were established in the right flank region of 42 female 6- to 8-wk-old nude mice (Charles River Laboratories, Inc.) by subcutaneous injection of 3×10^6 SKOV-3 cells in 50 μL of PBS. Tumors were allowed to grow to a mean maximum diameter of 4 mm (range, 3–8 mm).

Targeted Contrast-Enhanced Ultrasound Imaging. Two-dimensional fundamental brightness-mode (B-mode) targeted contrast-enhanced ultrasound imaging was performed with a dedicated small-animal high-resolution imaging system (Vevo 770; VisualSonics). A 40-MHz high-frequency linear transducer (real-time microvisualization [RMV] scan head 704 [VisualSonics]; lateral and axial resolutions of 100 and 40 μm, respectively; focal length, 6 mm; transmit power, 50%; mechanical index, 0.14; dynamic range, 52 dB) was fixed on a rail system, and the acoustic focus was centered at the level of the subcutaneous tumors. The mice were maintained anesthetized with 2% isoflurane in oxygen (2 L/min) during scanning. All imaging settings were kept constant throughout each imaging session.

In 19 tumor-bearing mice, 5×10^7 MB-Knottin$_{Integrin}$ and 5×10^7 MB$_{cRGD}$ were injected intravenously via the tail vein (microbubble volume per injection, 100 μL; injection time, 4 s) in random order during the same imaging session. In an additional 9 tumor-bearing mice, 5×10^7 MB-Knottin$_{Integrin}$ and 5×10^7 MB$_{\alpha v\beta 3}$ were injected intravenously in random order during the same imaging session. Between injections, an interval of 30 min was used to allow the clearance of microbubbles from the vasculature. After each injection, targeted contrast-enhanced ultrasound imaging was performed with the destruction–replenishment imaging sequence as described previously (*14–16*). In brief, 120 B-mode imaging frames were acquired over a 6-s period 4 min after each microbubble injection. Next, a continuous high-power destructive pulse (10 MHz; mechanical index, ~0.235; average power, ~0.0676 W/cm^2) was applied for 3 s to destroy all microbubbles within the beam elevation. At 9 s after destruction (to allow freely circulating microbubbles to refill tumor vessels), another 120 imaging frames were acquired. The imaging signals (video intensity) from these 120 imaging frames were averaged (to compensate for slight breathing motion artifacts) and digitally subtracted from the initial 120 (predestruction) frames. The resulting difference in video intensity corresponded to the imaging signal attributable to microbubbles adhering to endothelial cell molecular markers.

To test integrin-binding specificity, MB-Knottin$_{Integrin}$ and MB-Knottin$_{Scrambled}$ (negative control) were injected via the tail vein into a subgroup of 7 tumor-bearing mice in random order, and imaging was performed as described earlier. In addition, the hind limb adductor muscle was scanned as a tumor angiogenesis–negative model in these animals after the injection of MB-Knottin$_{Integrin}$ to assess the contrast enhancement of nonangiogenesis microvasculature (*15*). Between imaging experiments, an interval of 30 min was used to allow the clearance of microbubbles from the vasculature (*17,18*). Finally, in vivo blocking experiments were performed with an additional subgroup of 7 tumor-bearing mice to further test integrin-binding specificity. In these mice, 5×10^7 MB-Knottin$_{Integrin}$ were injected intravenously, and imaging was performed as described earlier. After 30 min to allow the clearance of microbubbles from the blood circulation, c(RGDyK) pentapeptide (0.5 μmol dissolved in 400 μL of PBS) was injected to block integrin receptors. After 30 min to allow the distribution of c(RGDyK), targeted ultrasound imaging with 5×10^7 MB-Knottin$_{Integrin}$ was repeated.

Image Analysis

Imaging frames were recorded digitally and analyzed offline with commercially available software (Vevo 770 high-resolution microultrasound imaging software; VisualSonics). Average image brightness (video intensity, which corresponds to the 8-bit log compressed gray scale) was measured in regions of interest drawn over the whole tumor on 2-dimensional imaging planes, and the difference in video intensities between predestruction and post-destruction image frames (see earlier description) was automatically displayed by the software as a colored (green) overlay on the B-mode anatomic images.

Ex Vivo Immunofluorescence Staining of Tumors

After ultrasound imaging, subcutaneous tumors were excised, embedded in optimum cutting temperature compound (O.C.T.; Sakura Finetek), frozen on dry ice, fixed with ice-cold acetone, and cut into 8-μm sections. Slices were incubated for 1 h in 5% goat serum to block nonspecific binding. For staining of mouse $\alpha_v\beta_3$ integrin, a hamster antimouse β_3 subunit primary antibody (1:100 dilution; BD Bioscience), a biotinylated mouse antihamster secondary antibody (1:300 dilution; BD Bioscience), and Alexa-Fluor 594-labeled streptavidin (1:200 dilution; Invitrogen) were used. Slices were doubly stained for mouse CD31 with a rat

antimouse CD31 primary antibody (1:100 dilution; BD PharMingen) and an AlexaFluor 488-labeled goat antirat secondary antibody (1:500 dilution; Jackson ImmunoResearch Laboratories). CD31 was used as a marker of vascular endothelial cells. Sections were mounted in aqueous mounting medium (Biomeda), and fluorescent images were acquired by microscopy (Axiophot; Carl Zeiss AG) and documented with a digital camera (AxioCam MRc; Carl Zeiss AG).

Statistical Analysis

Data are reported as mean ± SD. A 4 × 2 between-groups ANOVA was performed for rates of attachment of microbubbles to cells with fixed factors of contrast agent (MB-Knottin$_{Integrin}$, MB-Knottin$_{Scrambled}$, MB$_{cRGD}$, and MB$_{\alpha v\beta 3}$) and cell line (integrin-positive and integrin-negative cells). Differences in attachment of MB-Knottin$_{Integrin}$ to cells with and without adding blocking antibodies were assessed with the Mann–Whitney test. Differences in in vivo ultrasound imaging signals in animals injected with MB-Knottin$_{Integrin}$ and with other microbubbles (MB-Knottin$_{Scrambled}$, MB$_{cRGD}$, and MB$_{\alpha v\beta 3}$) were assessed with the paired Wilcoxon test. The paired Wilcoxon test was also used to test differences in signal intensities in in vivo blocking experiments and to test differences in signal intensities obtained in tumor xenografts and in nonangiogenic normal skeletal muscle tissue. All statistical analyses were done with Stata 9.2 (Stata Corp.). A P value of less than 0.05 was considered statistically significant. For the subgroup of 7 mice in which 2 comparisons were made (MB-Knottin$_{Integrin}$ vs. MB-Knottin$_{Scrambled}$ and MB-Knottin$_{Integrin}$ in tumor vs. hind limb adductor muscle), a Bonferroni adjustment was performed; a P value of less than 0.025 indicated significance. For the flow chamber experiments with 3 comparisons (MB-Knottin$_{Integrin}$ vs. MB-Knottin$_{Scrambled}$, MB$_{cRGD}$, and MB$_{\alpha v\beta 3}$), a P value of less than 0.016 was considered significant.

RESULTS

Flow Chamber Cell Attachment Studies

MB-Knottin$_{Integrin}$ attached significantly more (P = 0.0001) to integrin-positive cells (1.76 ± 0.49 microbubbles per cell) than to negative control cells (0.07 ± 0.006 microbubbles per cell) (Table 1). Control MB-Knottin$_{Scrambled}$ adhered significantly less (P = 0.002) to integrin-positive cells (0.15 ± 0.12 microbubbles per cell) than MB-Knottin$_{Integrin}$ (Fig. 1). After preblocking of integrins on integrin-positive cells with c(RGDyK) peptide, the attachment of MB-Knottin$_{Integrin}$ to these cells decreased significantly (P = 0.04) (Table 1).

[Table 1] [Fig. 1]

TABLE 1. Flow Chamber Cell Culture Attachment Studies with Different Types of Microbubbles

Cell line	Type of microbubble	No. of adherent microbubbles/cell	
		Mean	SD
Integrin-positive cells	MB-Knottin$_{Integrin}$	1.76	0.49
	MB-Knottin$_{Scrambled}$	0.15	0.12
	MB$_{\alpha v\beta 3}$	0.60	0.07
	MB$_{cRGD}$	0.74	0.32
	MB-Knottin$_{Integrin}$ after blocking	0.20	0.16
Integrin-negative cells	MB-Knottin$_{Integrin}$	0.07	0.006
	MB-Knottin$_{Scrambled}$	0.08	0.03
	MB$_{\alpha v\beta 3}$	0.13	0.11
	MB$_{cRGD}$	0.11	0.05

MB-Knottin$_{Integrin}$ = microbubbles targeted with $\alpha_v\beta_3$ integrin-binding knottin peptide; MB-Knottin$_{Scrambled}$ = microbubbles targeted with knottin peptide containing scrambled sequence; MB$_{\alpha v\beta 3}$ = microbubbles targeted with anti-$\alpha_v\beta_3$ integrin monoclonal antibody; MB$_{cRGD}$ = microbubbles targeted with $\alpha_v\beta_3$ integrin-binding pentapeptide c(RGDfK).

Blocking was done by preincubation of integrin-positive cells with c(RGDyK) (1.25 μmol/μL).

Small-Animal Imaging Experiments

In the group of tumor-bearing mice that were imaged with both MB-Knottin$_{Integrin}$ and MB$_{\alpha v\beta 3}$ in the same imaging session, the imaging signal was significantly higher (P = 0.009) after the administration of MB-Knottin$_{Integrin}$ (11.9 ± 6.1) than after the administration of MB$_{\alpha v\beta 3}$ (5.6 ± 2.3) (Fig. 2). The imaging signals following MB-Knottin$_{Integrin}$ administration (9.1 ± 6.4) and following MB$_{cRGD}$ administration (7.1 ± 7.9) were not statistically significant different (P = 0.117).

[Fig. 2]

To confirm the specificity of MB-Knottin$_{Integrin}$ binding to $\alpha_v\beta_3$ integrin, MB-Knottin$_{Scrambled}$ were administered to another group of tumor-bearing mice. The imaging signal was significantly lower (P = 0.018) after the administration of MB-Knottin$_{Scrambled}$ (control) (5.2 ± 1.0) than after the administration of MB-Knottin$_{Integrin}$ (15.5 ± 5.6) (Fig. 3). To further confirm the $\alpha_v\beta_3$ integrin-binding specificity of MB-Knottin$_{Integrin}$, in vivo blocking experiments were performed with another group of tumor-bearing mice. After in vivo blocking of integrin receptors with c(RGDyk) peptide, the imaging signal after the administration of MB-Knottin$_{Integrin}$ decreased significantly (P = 0.018), from 13.2 ± 7.0 before blocking to 4.7 ± 4.0 after blocking (Fig. 4). Finally, as a quasi negative control for nonangiogenic vessels, hind limb muscles were also imaged with targeted contrast-enhanced ultrasound imaging after the intravenous administration of MB-Knottin$_{Integrin}$. The imaging signal in these experiments was significantly lower (1.3 ± 0.3) (P = 0.018) than that in the angiogenic tumor tissues. In vivo imaging data are summarized in Table 2.

[Fig. 3] [Fig. 4] [Table 2]

Ex Vivo Immunofluorescence Staining of Tumors

Immunofluorescence showed colocalization of the β_3 subunit with CD31, confirming the presence of mouse $\alpha_v\beta_3$ integrin on angiogenic endothelial cells within the SKOV-3 tumors used in this study (Fig. 5).

[Fig. 5]

DISCUSSION

In this proof-of-principle study, we have demonstrated that tumor angiogenic vessels can be visualized by targeted contrast-enhanced ultrasound imaging using contrast

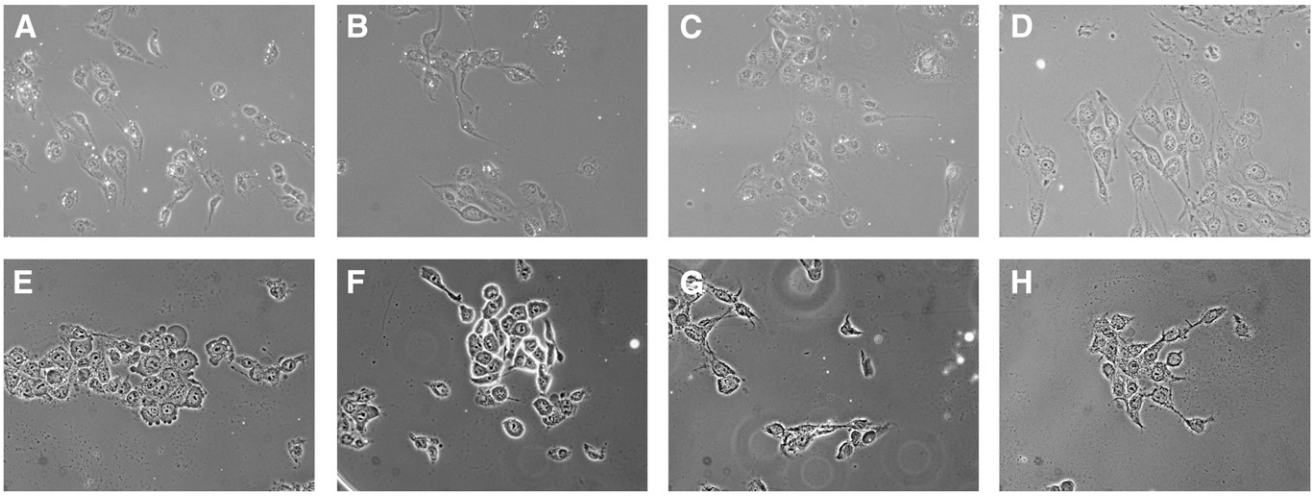

FIGURE 1. Representative images of integrin-positive (A–D) and integrin-negative (E–H) cells exposed to MB-Knottin$_{Integrin}$ (A and E), MB$_{cRGD}$ (B and F), MB$_{\alpha v\beta 3}$ (C and G), and MB-Knottin$_{Scrambled}$ (D and H) under flow shear stress conditions in flow chamber cell culture attachment studies. Microbubbles are small, rounded white structures.

microbubbles (MB-Knottin$_{Integrin}$) targeted with a new, small integrin-binding knottin peptide. The in vivo targeted contrast-enhanced ultrasound imaging signal with MB-Knottin$_{Integrin}$ was similar to or higher than that obtained with a previously reported ultrasound contrast agent functionalized with c(RGDfK) or a monoclonal antibody, respectively (*8,9*). These data have implications for the development of knottin peptides as ligands for novel microbubble-targeted contrast agents for noninvasive imaging of tumor angiogenesis with targeted contrast-enhanced ultrasound imaging.

Targeted contrast-enhanced ultrasound imaging is currently being evaluated for the visualization of tumor angiogenesis by use of targeted contrast microbubbles conjugated to various types of ligands that bind to molecular markers of angiogenesis, including vascular endothelial growth factor receptor type 2, endoglin, or integrins (*7–9,16,19–21*). In this work, we tested whether knottin peptides could be used as a new class of integrin-binding ligands for targeted contrast-enhanced ultrasound imaging, with the idea that if successful, this study would provide proof-of-concept for engineering knottin peptides against biologic markers of angiogenesis beyond $\alpha_v\beta_3$ integrins for targeted contrast-enhanced ultrasound imaging of tumor angiogenesis. Knottin peptides are small peptides that consist of a core of at least 3 disulfide bonds that are interwoven into a "knotted" conformation (*10*). These "miniproteins" are promising molecular scaffolds for protein engineering because their family members share little sequence homology apart from their core cysteine residues. Knottins have great potential for in vivo applications due to their resistance to proteolysis and their high thermal stability (*22*). In addition, this class of molecules is thought to be nonimmunogenic (*23,24*). Because of their small size, knottin peptides can be produced by solid-phase synthesis, allowing chemical handles to be introduced for site-specific

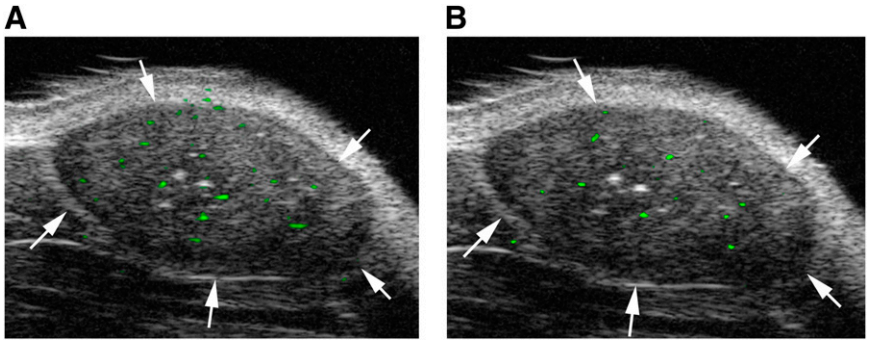

FIGURE 2. Targeted contrast-enhanced ultrasound imaging with MB-Knottin$_{Integrin}$ (A) and MB$_{\alpha v\beta 3}$ (B) in nude mouse with subcutaneous human ovarian adenocarcinoma xenograft tumor (arrows). Two-dimensional ultrasound imaging was performed in same session, with 30 min between injections to allow clearance of previously injected microbubbles. Molecular imaging signal from attached microbubbles is color coded as green signal overlaid on gray scale ultrasound image and was higher after MB-Knottin$_{Integrin}$ injection than after MB$_{\alpha v\beta 3}$ injection in this tumor. Because subcutaneous human ovarian cancer xenograft tumors are poorly vascularized, only low, but substantial, targeted contrast-enhanced ultrasound imaging signal can be measured. In addition, low signal is visible at tumor boundaries, most likely from microbubbles attached to angiogenic vessels in tissue surrounding tumor.

RGB

jnm068007-pe ■ 2/5/10

RGB

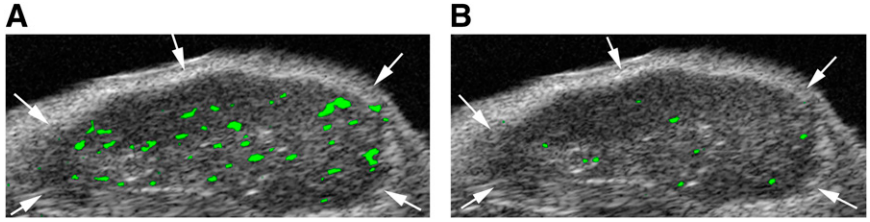

FIGURE 3. Subcutaneous human ovarian adenocarcinoma xenograft tumor (arrows) imaged with targeted contrast-enhanced ultrasound imaging after intravenous injection of MB-Knottin$_{Integrin}$ (A) and MB-Knottin$_{Scrambled}$ (control) (B). Imaging signal obtained after MB-Knottin$_{Integrin}$ injection was substantially higher than that obtained after MB-Knottin$_{Scrambled}$ (control) injection.

conjugation to the shell of ultrasound contrast microbubbles.

There is limited experience in using novel peptides as binding ligands to assess tumor angiogenesis with targeted contrast-enhanced ultrasound imaging. With an in vitro bacterial peptide display library panned against tumor cells derived from SCC-VII murine squamous cell carcinomas, a cyclic peptide containing the tripeptide sequence RRL was identified as a tumor endothelial cell–specific binding peptide (*25*). This peptide was conjugated to the shell of contrast microbubbles and used for in vivo targeted contrast-enhanced ultrasound imaging of tumor angiogenesis (*15*). In that study (*15*), the in vivo ultrasound imaging signal in subcutaneous human pancreatic cancer xenografts was substantially higher after intravenous administration of RRL-labeled microbubbles than after administration of control peptides, suggesting that the RRL-containing imaging probe allows visualization and quantification of tumor angiogenesis (*15*). However, the molecular target on tumor endothelial cells for the tumor-binding peptide RRL is not yet known (*15*).

In our proof-of-principle study, we chose to use a binding ligand to the well-characterized angiogenesis marker $\alpha_v\beta_3$ integrin to test the feasibility of using knottin peptides for targeting targeted contrast-enhanced ultrasound imaging contrast agents. Cell culture binding experiments showed substantially higher binding of MB-Knottin$_{Integrin}$ to the surface of integrin-positive cells than to negative control cells. Binding to integrin-positive cells could be blocked by preincubating the cells with c(RGDyK) peptide, further confirming binding specificity of MB-Knottin$_{Integrin}$ to $\alpha_v\beta_3$ integrin. In vivo, there was a similar trend in small-animal targeted contrast-enhanced ultrasound imaging experiments. The imaging signal was substantially higher in angiogenic tumor vessels in tumor xenografts compared with nonangiogenic negative control vessels in hind limb muscle tissues. In addition, binding specificity of our imaging agent was further confirmed by in vivo blocking studies, as well as by injecting microbubbles functionalized with a knottin peptide containing a scrambled integrin-binding sequence (MB-Knottin$_{Scrambled}$). In both control experiments, the ultrasound imaging signal was substantially lower than the imaging signal after MB-Knottin$_{Integrin}$ injection. Finally, ex vivo immunofluorescence staining confirmed $\alpha_v\beta_3$ integrin expression on angiogenic tumor vessels in human ovarian adenocarcinoma xenograft tumors in mice.

We also compared the in vivo targeted contrast-enhanced ultrasound imaging signal after MB-Knottin$_{Integrin}$ injection with microbubbles functionalized with either c(RGDfK) (MB$_{cRGD}$), or a monoclonal antibody against the α_v subunit of $\alpha_v\beta_3$ (MB$_{\alpha v\beta 3}$). On average, the imaging signal after MB-Knottin$_{Integrin}$ administration was higher compared with both types of microbubbles, but reached statistical significance only when compared with MB$_{\alpha v\beta 3}$. In general, several factors may influence the binding of contrast microbubbles to molecular targets expressed on tumor endothelial cells, including the extent of tumor vascularization (e.g., perfused vs. necrotic parts of the tumor), physical forces that translate the freely circulating microbubbles to the vessel wall, and the density of the expressed target on tumor vessels. Moreover, the properties of the target–ligand interactions are also important, such as the affinity of the nonconjugated binding ligand to the molec-

RGB

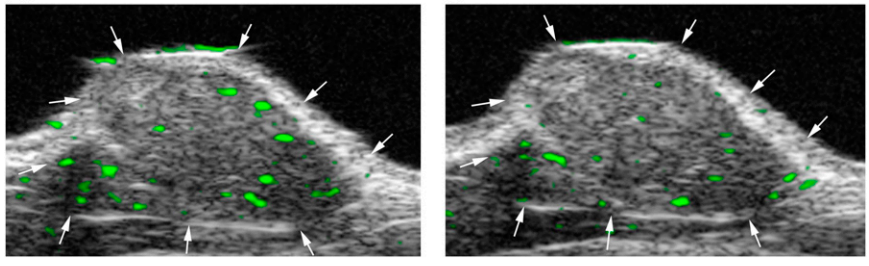

FIGURE 4. Transverse color-coded ultrasonic images of subcutaneous human ovarian adenocarcinoma xenograft tumor (arrows) in nude mouse. Imaging with MB-Knottin$_{Integrin}$ was performed before (A) and 30 min after (B) intravenous administration of blocking c(RGDyK). Targeted contrast-enhanced ultrasound imaging signal, shown as green signal overlaid on gray scale image, was substantially reduced after administration of blocking peptide. Low signal is visible at tumor boundaries, most likely from microbubbles attached to angiogenic vessels in tissue surrounding tumor.

TABLE 2. In Vivo Imaging Signals (Expressed as Video Intensities) Obtained with Different Types of Microbubbles in SKOV-3 Tumors and Muscle in Mice

Type of microbubble	Mean ± SD video intensity in study: 1 (SKOV-3 tumors)	2 (SKOV-3 tumors)	3 (SKOV-3 tumors)	4 (SKOV-3 tumors)	5 (Muscle)
MB-Knottin$_{Integrin}$	11.9 ± 6.1	9.1 ± 6.4	15.5 ± 5.6	13.2 ± 7.0	1.3 ± 0.3*
MB$_{\alpha v\beta 3}$	5.6 ± 2.3†				
MB$_{cRGD}$		7.1 ± 7.9‡			
MB-Knottin$_{Scrambled}$			5.2 ± 1.0*		
MB-Knottin$_{Integrin}$ after blocking				4.7 ± 4.0*	

*$P < 0.05$.
†$P < 0.01$.
‡Not significant.
SKOV-3 = human ovarian adenocarcinoma xenograft; muscle = hind limb muscle tissue (control).

ular target, as well as the avidity of the ligand–microbubble complex to the molecular target. In a recent study, the impact of ligand affinity on immunoliposome nanoparticles targeted to the epidermal growth factor receptor (EGFR) was studied in cell culture experiments (*26*). With directed evolution, single-chain antibody fragments with different EGFR-binding affinities were identified, and the effects of targeted nanoparticles coupled to these antibody fragments on EGFR-expressing tumor cells were studied. With nanoparticles containing high surface densities of antibody fragments, there was no substantial impact of the respective affinity of the antibody fragments (with affinities ranging from 264 to 0.9 nM) on the overall binding of the nanoparticles to EGFR-expressing tumor cells (*26*). These findings may be explained by an increased functional affinity (i.e., avidity) of the particles due to the conjoint interaction of multiple binding ligands. Although the reported affinity of monomeric cyclic RGD-based ligands to $\alpha_v\beta_3$ integrins is weaker than the affinity of the Knottin$_{Integrin}$ peptide—with a 50% inhibitory concentration of about 100 nM for c(RGDfK) vs. a 50% inhibitory concentration of about 20 nM for Knottin$_{Integrin}$ (*12,27*)—increased avidity from multiple binding ligands may explain the comparable results of MB$_{cRGD}$ and MB-Knottin$_{Integrin}$ both in cell cultures and in small-animal in vivo experiments in our study. Interestingly, the imaging signal of MB$_{\alpha v\beta 3}$ was substantially lower than that of MB-Knottin$_{Integrin}$, although the affinities of nonconjugated monoclonal antibodies and Knottin$_{Integrin}$ are similar (*12*). Additional factors, such as the geometry or size of binding ligands on the shell of microbubbles (e.g., monoclonal antibodies have a size of ~150 kDa; Knottin$_{Integrin}$ has a size of ~3 kDa), may have an influence on the overall binding capacity of the targeted microbubbles used in our study. Further studies are warranted to test this hypothesis.

The following limitations of our study need to be addressed. We did not perform an intraindividual comparison of different microbubbles (MB-Knottin$_{Integrin}$, MB$_{cRGD}$, MB$_{\alpha v\beta 3}$, MB-Knottin$_{Scrambled}$) in the same animals in the same imaging session. To keep the imaging time of each animal reasonably short we tested the novel MB-Knottin$_{Integrin}$ in different groups of tumor-bearing animals. This approach reduced possible interactions from still circulating microbubbles from previous injections after repetitive injections of different types of microbubbles. As discussed earlier, the imaging signal after injection of targeted microbubbles depends on various factors, including the extent of tumor vascularization (e.g., perfused

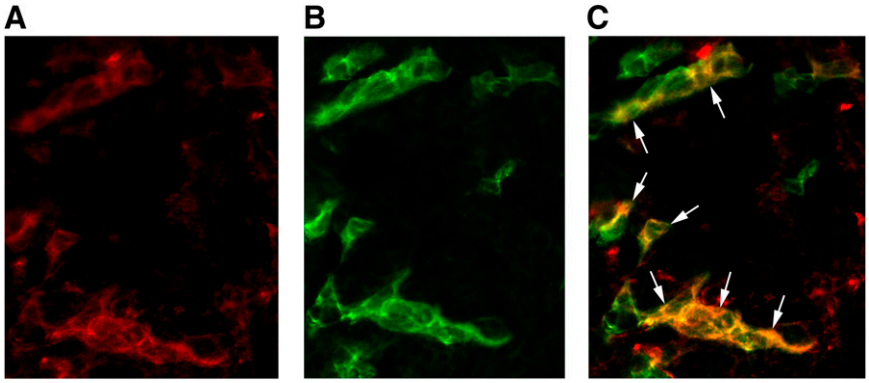

FIGURE 5. Micrograph of frozen human ovarian adenocarcinoma xenograft tumor tissue slices after immunofluorescence staining for both β_3 integrin subunit (A) and CD31 (B). CD31 was used as marker of tumor endothelial cells. Immunofluorescence images show tissue staining of mouse β_3 integrin subunit (red color) and mouse CD31 (green color). Image resulting from merging of those images (staining of β_3 integrin subunit and CD31) (C) demonstrates that β_3 integrin subunit is localized on tumor vessel endothelial cells (arrows; yellow on image resulting from merging confirms colocalization). β_3 integrin was visualized with AlexaFluor 594 (red), and CD31 was visualized with AlexaFluor 488 (green). Original magnification, ×400.

RGB

vs. necrotic parts of the tumor) and the profiles of expression of the target $\alpha_v\beta_3$ integrin on tumor endothelial cells. The fact that MB-Knottin$_{Integrin}$ was tested in different groups of animals with various sizes of tumors in our study may explain the difference in the mean imaging signal after MB-Knottin$_{Integrin}$ injection in our study. Although this was not the focus of our study, future studies are needed to correlate targeted contrast-enhanced ultrasound imaging signal after MB-Knottin$_{Integrin}$ injection and levels of $\alpha_v\beta_3$ integrin expression to further confirm this hypothesis. Furthermore, the ultrasound imaging system (Vevo 770) used in the present study allowed imaging only in the fundamental mode, and nonlinear scanning with substantial suppression of background signal was not possible with this imaging system. This may account for the relatively low overall imaging signal from bound contrast microbubbles in the tumor xenografts in this study. Finally, for this proof-of-principle study, streptavidin–biotin interactions were used to couple knottin peptides onto the surface of contrast microbubbles. Because streptavidin is immunogenic and can cause severe allergic reactions in patients, alternative binding chemistries will be needed for coupling knottin peptides onto the microbubble shell for future clinical translation.

CONCLUSION

The results of our study suggest that knottin peptide–based contrast microbubbles can be created and successfully used for targeted contrast-enhanced ultrasound imaging of integrins in the tumor vasculature. Because knottin peptides have the potential to be engineered as binding ligands for a variety of different biologic markers of angiogenesis beyond $\alpha_v\beta_3$ integrins, this work opens a pathway toward the development of future novel targeted contrast-enhanced ultrasound imaging agents.

ACKNOWLEDGMENTS

We are very grateful to Jarrett Rosenberg for his help with the statistical analysis of the data in this study. This work was supported by RSNA seed grant RSD0809, the Howard S. Stern research grant from the Society of Gastrointestinal Radiologists, NCI ICMIC developmental grant CA114747 P50, NIH grant R21 CA139279, NCI grant 5K01 CA104706, the Edward Mallinckrodt, Jr., Foundation, and the Canary Foundation.

REFERENCES

1. Willmann JK, van Bruggen N, Dinkelborg LM, Gambhir SS. Molecular imaging in drug development. *Nat Rev Drug Discov.* 2008;7:591–607.
2. Lindner JR. Microbubbles in medical imaging: current applications and future directions. *Nat Rev Drug Discov.* 2004;3:527–532.
3. Folkman J. Angiogenesis. *Annu Rev Med.* 2006;57:1–18.
4. Hanahan D, Weinberg RA. The hallmarks of cancer. *Cell.* 2000;100:57–70.
5. Hood JD, Cheresh DA. Role of integrins in cell invasion and migration. *Nat Rev Cancer.* 2002;2:91–100.
6. Stupack DG, Cheresh DA. Integrins and angiogenesis. *Curr Top Dev Biol.* 2004;64:207–238.
7. Ellegala DB, Leong-Poi H, Carpenter JE, et al. Imaging tumor angiogenesis with contrast ultrasound and microbubbles targeted to alpha(v)beta3. *Circulation.* 2003;108:336–341.
8. Palmowski M, Huppert J, Ladewig G, et al. Molecular profiling of angiogenesis with targeted ultrasound imaging: early assessment of antiangiogenic therapy effects. *Mol Cancer Ther.* 2008;7:101–109.
9. Willmann JK, Lutz AM, Paulmurugan R, et al. Dual-targeted contrast agent for US assessment of tumor angiogenesis in vivo. *Radiology.* 2008;248:936–944.
10. Kolmar H. Alternative binding proteins: biological activity and therapeutic potential of cystine-knot miniproteins. *FEBS J.* 2008;275:2684–2690.
11. Favel A, Mattras H, Coletti-Previero MA, Zwilling R, Robinson EA, Castro B. Protease inhibitors from *Ecballium elaterium* seeds. *Int J Pept Protein Res.* 1989;33:202–208.
12. Kimura RH, Levin AM, Cochran FV, Cochran JR. Engineered cystine knot peptides that bind alphavbeta3, alphavbeta5, and alpha5beta1 integrins with low-nanomolar affinity. *Proteins.* 2009;77:359–369.
13. Villanueva FS, Jankowski RJ, Klibanov S, et al. Microbubbles targeted to intercellular adhesion molecule-1 bind to activated coronary artery endothelial cells. *Circulation.* 1998;98:1–5.
14. Lindner JR, Song J, Xu F, et al. Noninvasive ultrasound imaging of inflammation using microbubbles targeted to activated leukocytes. *Circulation.* 2000;102:2745–2750.
15. Weller GE, Wong MK, Modzelewski RA, et al. Ultrasonic imaging of tumor angiogenesis using contrast microbubbles targeted via the tumor-binding peptide arginine-arginine-leucine. *Cancer Res.* 2005;65:533–539.
16. Willmann JK, Paulmurugan R, Chen K, et al. US imaging of tumor angiogenesis with microbubbles targeted to vascular endothelial growth factor receptor type 2 in mice. *Radiology.* 2008;246:508–518.
17. Palmowski M, Morgenstern B, Hauff P, et al. Pharmacodynamics of streptavidin-coated cyanoacrylate microbubbles designed for molecular ultrasound imaging. *Invest Radiol.* 2008;43:162–169.
18. Willmann JK, Cheng Z, Davis C, et al. Targeted microbubbles for imaging tumor angiogenesis: assessment of whole-body biodistribution with dynamic micro-PET in mice. *Radiology.* 2008;249:212–219.
19. Korpanty G, Carbon JG, Grayburn PA, Fleming JB, Brekken RA. Monitoring response to anticancer therapy by targeting microbubbles to tumor vasculature. *Clin Cancer Res.* 2007;13:323–330.
20. Lyshchik A, Fleischer AC, Huamani J, Hallahan DE, Brissova M, Gore JC. Molecular imaging of vascular endothelial growth factor receptor 2 expression using targeted contrast-enhanced high-frequency ultrasonography. *J Ultrasound Med.* 2007;26:1575–1586.
21. Rychak JJ, Graba J, Cheung AM, et al. Microultrasound molecular imaging of vascular endothelial growth factor receptor 2 in a mouse model of tumor angiogenesis. *Mol Imaging.* 2007;6:289–296.
22. Craik DJ, Clark RJ, Daly NL. Potential therapeutic applications of the cyclotides and related cystine knot mini-proteins. *Expert Opin Investig Drugs.* 2007;16:595–604.
23. Chiche L, Heitz A, Gelly JC, et al. Squash inhibitors: from structural motifs to macrocyclic knottins. *Curr Protein Pept Sci.* 2004;5:341–349.
24. Maillere B, Mourier G, Herve M, Cotton J, Leroy S, Menez A. Immunogenicity of a disulfide-containing neurotoxin: presentation to T-cells requires a reduction step. *Toxicon.* 1995;33:475–482.
25. Brown CK, Modzelewski RA, Johnson CS, Wong MK. A novel approach for the identification of unique tumor vasculature binding peptides using an *E. coli* peptide display library. *Ann Surg Oncol.* 2000;7:743–749.
26. Zhou Y, Drummond DC, Zou H, et al. Impact of single-chain Fv antibody fragment affinity on nanoparticle targeting of epidermal growth factor receptor-expressing tumor cells. *J Mol Biol.* 2007;371:934–947.
27. Dijkgraaf I, Kruijtzer JA, Liu S, et al. Improved targeting of the alpha(v)beta (3) integrin by multimerisation of RGD peptides. *Eur J Nucl Med Mol Imaging.* 2007;34:267–273.